# The Role of Intercritical Annealing in Enhancing Low-temperature Toughness of Fe-C-Mn-Ni-Cu Structural Steel

XIAOHUI XI, JINLIANG WANG, XING LI, LIQING CHEN, and ZHAODONG WANG

In this article, an intercritical annealing (IA) process was introduced to the conventional quenching and tempering (QT) heat treatment for a Fe-C-Mn-Ni-Cu structural steel. The corresponding microstructures and mechanical properties of this steel were characterized by scanning electron microscope (SEM) equipped with electron back scattering diffraction (EBSD) and mechanical properties test. The results showed that IA process could lead to a considerable increase in low-temperature toughness for this steel. A mixed microstructure was obtained after IA process had been adopted containing intercritical ferrite and tempered martensite together with a small amount of retained austenite. This steel with mixed microstructure exhibited tensile strength of 961 MPa, relatively lower yield strength of 830 MPa, and a lower yield-to-tensile ratio ($Y/T$ ratio) of 0.86, while a higher total elongation of 22.2 pct was achieved. The reason for this could be attributed to the multiple effect of multi-phase microstructure and deformation-induced transformation of the retained austenite during tensile deformation. The excellent low-temperature toughness was characterized by the Charpy impact energy as 183 J at 153 K ($-$ 120 °C), which was associated with highly stable retained austenite and finer microstructure through reversed transformation during intercritical annealing treatment. These can be considered to increase the resistance to crack initiation and propagation and decrease the ductile-brittle transformation temperature (DBTT).

## I. INTRODUCTION

HIGH-STRENGTH low-alloyed steels with improved low-temperature toughness and good weldability are preferred as constructional materials for offshore structures, bridges, ship hull, and pressure vessels.[1–3] In regard to alloy design, low-carbon design is preferentially adopted for consideration of weldability and low-temperature toughness. Moreover, micro-alloying elements, such as Nb, V, and Ti, are usually added for carbide formation with aim to precipitation strengthening.[4–6] Cu is added to compensate for the loss of strength due to carbon reduction.[7] Additionally, Cu is helpful to improve the corrosion resistance of the marine structural steels.[8] Although a balance of strength, ductility, toughness, and weldability has been obtained in structural steels, higher requirements for strength–toughness combination are proposed due to their severer service conditions, stricter demands for safety and reliability, long-term service, etc.

In order to meet the requirement for higher performance, numerous approaches have been developed for various alloying steels, such as the addition of alloy elements, thermal mechanical controlled processing (TMCP), and heat treatments.[1,9,10] Presently, one of the most effective heat treatments is quenching and tempering in the production of ultrahigh-strength steels.[11] The quenching process is a common way to increase the strength of high-strength steels by generating a high density of dislocations in martensite, which are obtained during the rapidly cooling to room temperature after reheating hot-rolled steels to the austenization temperature.[12] The subsequent tempering process can improve the toughness of the quenched steels by relaxing dislocations,[13] accompanied with the loss of strength, which is attributed to the intrinsic conflict between strength and toughness. Meanwhile, the brittle cementite is inevitable to precipitate during conventional quenching and tempering, causing initial cracks and thus decreasing the low-temperature toughness.[14] Another problem to be solved for high-strength steels is the high yield-to-tensile ratio ($Y/T$ ratio). It has

XIAOHUI XI, JINLIANG WANG, XING LI, LIQING CHEN, and ZHAODONG WANG are with the State Key Laboratory of Rolling and Automation, Northeastern University, 3-11 Wenhua Road, Shenyang 110819, P.R. China. Contact e-mail: lqchen@mail.neu.edu.cn

been found that the $Y/T$ ratio increases with the increase of yield strength.[1,12,15,16] When the yield strength is higher than 690 MPa, the $Y/T$ ratio increases up to 0.9 or more. However, the higher $Y/T$ ratio definitely means the poorer formability, which seriously limits the industrial application of ultrahigh-strength steels.

Intercritical annealing has been demonstrated as a new method capable of producing multi-phase microstructure in low-carbon steels, which are characterized by high strength, ductility, and toughness. Therefore, the intercritical annealing has long been receiving more and more attentions. The intercritical annealing is generally carried out by heating steels into the two-phase ($\alpha + \gamma$) region for soaking, during which alloying elements such as carbon, manganese, and nickel are redistributed between the matrix and the reverted austenite. This results in the mixed microstructure of intercritical ferrite and element-enriched reversed austenite. During subsequent cooling, the reverted austenite transforms to martensite or bainite, or keeps till to room temperature, depending on the chemical compositions and cooling rates.

Over the past few years, plenty of investigations have been directed toward microstructural characterization and mechanical properties in the intercritical annealing process. On the one hand, the intercritical annealing was applied to develop ferrite-martensite dual-phase steels based on conventional high-strength low-alloy (HSLA) steels.[17] Due to the particular microstructure in which soft ferrite provided good ductility, while hard martensite guaranteed strength, a good combination of strength and ductility was achieved. Besides these features, high work hardening rate, high toughness, and uniform plastic deformation were also present. On the other hand, the intercritical annealing has been widely used to create retained austenite. Shi *et al.*[18] developed a 0.2C-7Mn steel with more than 30 pct retained austenite *via* intercritical annealing. A high tensile strength of 1420 MPa with a high total elongation of about 31 pct was obtained. This can be explained by the strain-induced phase transformation from metastable retained austenite. The intercritical annealing was also employed in a 5.5 pctNi cryogenic steel to obtain a dense distribution of the thermally stable austenite.[19] An excellent low-temperature toughness of about 140 J at 233 K (− 40 °C) was achieved without loss of strength and ductility. In the aforementioned high-alloyed (Ni ≥ 5 pct, Mn ≥ 5 pct) steels, the retained austenite can be stabilized by partitioning of austenite stabilizers (Ni, Mn) during intercritical annealing.[19,20] Thus, an excellent combination of strength, ductility, and toughness was obtained through transformation-induced plasticity (TRIP) of the retained austenite. However, it seems difficult to obtain some amount of retained austenite in low-carbon (C ≤ 0.1 pct) steels with low alloying elements, such as low -alloyed steels with Mn less than 2 pct or/and Ni less than 3 pct.

The aim of the present study is to examine the effect of intercritical annealing on the microstructural evolution and mechanical properties of a Fe-C-Mn-Ni-Cu structural steel with low carbon and low alloying elements. So, the intercritical annealing was introduced to the conventional quenching and tempering (QT) processes to obtain multi-phase microstructures with considerable amount of retained austenite. And the mechanical properties of this structural steel were evaluated, especially the low-temperature toughness. The toughening mechanism of this steel subjected to intercritical annealing was disclosed on the basis of the retained austenite stability and grain refinement, together with a comparison to the conventional QT treatment.

## II. EXPERIMENTAL

The steel used in this study has a normally chemical composition of 0.08C-0.24Si-1Mn-2.5Ni-1.5-Cu-0.54Cr-0.55Mo-0.03Nb-0.05V (in wt pct) and Fe balanced. The steel was initially smelted in a vacuum induction furnace (50 Kg capacity). The ingots were then forged into rectangular slabs with a cross section of 100 mm × 120 mm. The slabs were reheated to 1473 K (1200 °C) for 2 hours and finally hot rolled to 24 mm in 7 passes. The samples for heat treatments were cut along rolling direction and the size is 120 mm × 30 mm × 24 mm.

The steel samples were firstly homogenized at 1123 K (850 °C) for 1 hour, followed by quenching to room temperature. They were divided into two groups and one group was directly tempered at 893 K (620 °C), designated as T620, while the other was subjected to intercritical annealing at 973 K (700 °C) for 1 hour and then tempering at 893 K (620 °C) for 1 hour, which was denoted as IA700-IT620. Figure 1 shows the schematics of the heat treatments.

The samples for microstructural observation were prepared by mechanical polishing and etching in a 4 pct (in vol pct) nital solution. The SEM microstructures were characterized on a ZEISS ULTRA-55 field emission scanning electron microscope (FE-SEM) at an acceleration voltage of 15 kV. The EBSD samples were prepared by electro-polishing in a 12.5 pct (in vol pct) perchloric acid solution at 18 V for 18 seconds to release surface stress and subsequently observed at an acceleration voltage of 20 kV and a scanning step of 0.15 $\mu$m.

The procedure of XRD samples preparation was the same as that for EBSD observation. The XRD profiles of the retained austenite were measured in D8 Discover X-ray diffractometer with CoK$\alpha$ radiation at a scanning speed of 2 deg/min. The volume fraction of retained austenite was calculated based on the integrated intensities of the (200)$\gamma$, (220)$\gamma$, (311)$\gamma$, (200)$\alpha$, and (211)$\alpha$ diffraction peaks according to Eq. [1].[21]

$$V_\gamma = 1.4 I_\gamma / (I_\alpha + 1.4 I_\gamma). \qquad [1]$$

The cylindrical tensile specimens with gage size of $\phi$ 5 mm × 50 mm were machined from the heat -treated plates and the tensile direction was parallel to the rolling direction. The room-temperature mechanical properties in terms of strength and elongation were measured on CMT5105 Instron test machine and the crosshead speed was 3 mm/min. The Charpy V-notch impact test was

conducted by adopting standard specimens of 10 mm × 10 mm × 55 mm in a wide temperature range of 77 K ~ 288 K (− 196 °C ~ 15 °C). The fractured surface morphologies were observed by SEM.

## III.  RESULTS AND DISCUSSION

### A. *Microstructure Features*

Figure 2 shows the SEM images of this Cu-containing steel heat treated by different processes. The microstructural evolution of this steel subjected to conventional quenching and tempering are presented in Figures 2(a) and (b). As observed in Figure 2(a), the microstructure of this steel contained a great deal of lath martensite after quenching. The initial lath martensite obtained after pre-quenching determines the distribution and morphology of subsequent structure during intercritical annealing and tempering.[22] When the quenched steel was directly tempered at 893 K (620 °C), the typical tempered martensite was obtained, as shown in Figure 2(b). Some of the lath boundaries disappeared in the as-quenched martensite as manifested by larger more uniformly etched areas. The reserved boundaries were ambiguous due to the recovery of martensite in the tempering process. The microstructural features of the steel subjected to quenching, intercritical annealing, and
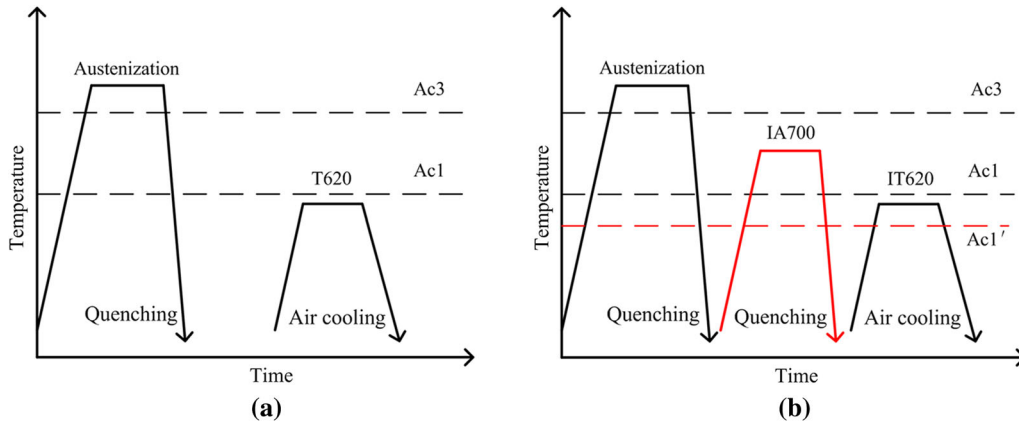


Fig. 1—Schematics of the conventional quenching and tempering (*a*) T620 and intercritical heat treatment (*b*) IA700-IT620.
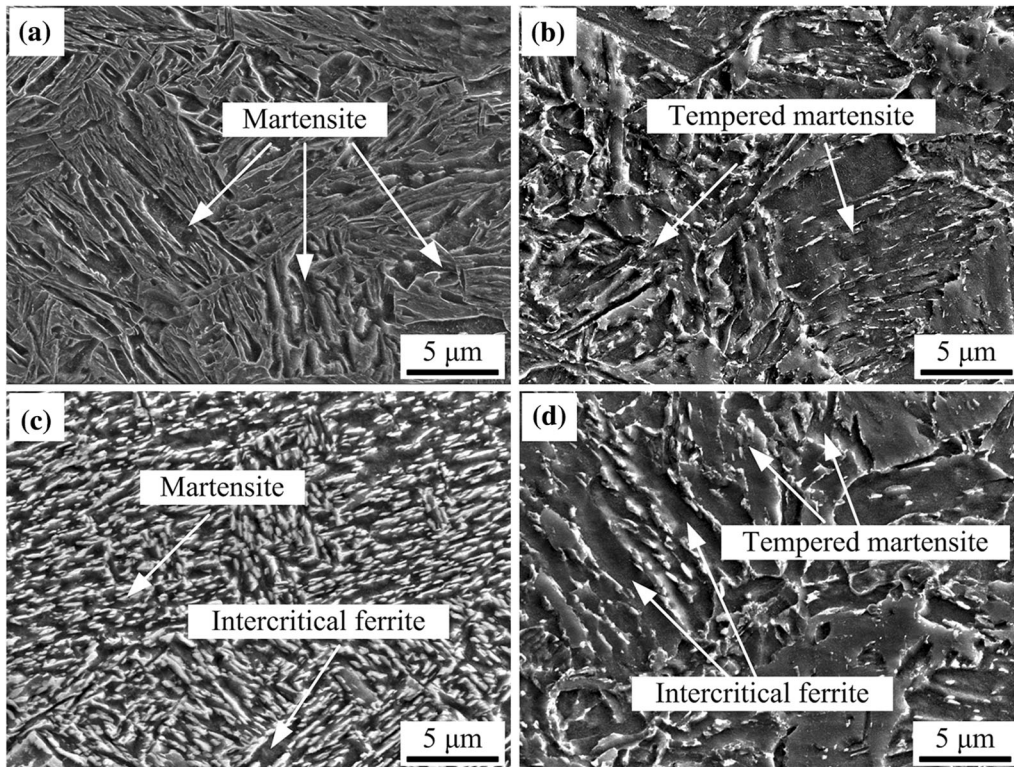


Fig. 2—SEM micrographs of Fe-C-Mn-Ni-Cu steel subjected to various heat treatments: (*a*) as quenched; (*b*) T620; (*c*) IA700; (*d*) IA700-IT620.

tempering are depicted in Figures 2(a), (c), and (d), respectively. As compared with the microstructure of the steel after conventional quenching and tempering, as shown in Figure 2(c), a dual-phase structure consisting of intercritical ferrite and newly formed martensite was observed in the steel after intercritical annealing at 973 K (700 °C). In this case, the martensite had much smaller size than that of the quenched steel due to austenite reversed transformation from martensite. When the intercritically annealed steel was followed by a tempering at 893 K (620 °C), a mixed microstructure was produced, as shown in Figure 2(d). In this stage, the newly formed martensite during intercritical annealing experienced recovery. Also, the fine intercritical ferrite coalesced with each other and finally existed as blocky. In addition to the intercritical ferrite and tempered martensite, some fine laminar structure was also present dispersedly in the matrix and at the boundaries. Based on the previous study,[23] the fine laminar structure may be some small amount of retained austenite. However, due to its subsize and the limited resolution of SEM, it was difficult to be distinguished from SEM micrographs. As a whole, the multi-phase microstructure consisting of intercritical ferrite, tempered martensite, as well as some retained austenite was obtained by adopting intercritical annealing between the conventional quenching and tempering.

In order to characterize the formation and distribution of the retained austenite in the steels under different conditions, the EBSD technique was used. Figure 3 shows the band contrast (BC) maps with face-center-cubic (FCC) phase under different heat treatments, in which the gray and red parts correspond to body-center-cubic (BCC) and FCC phases, respectively. The variations in brightness for gray phases indicate different BC values. Figure 3(a) presents more dark areas, indicating relatively low BC value. This was caused by the martensite with high density of dislocations after quenching. After subsequent tempering at 893 K (620 °C), some equiaxed grains were visible as seen from Figure 3(b). However, no retained austenite was observed. As shown in Figure 3(c), when the quenched steel was intercritically annealed at 973 K (700 °C), the retained austenite was dispersedly distributed in the matrix. Under this condition, stabilizing elements such as Ni, Mn, and C were redistributed while holding at the two-phase region, resulting in the formation of element-enriched reversed austenite and lean-alloyed ferrite. Once cooling, the reversed austenite transformed to martensite or retained austenite.[24] Meanwhile, the transus temperature of reverted austenite ($A_{c1}$) for alloy-enriched regions was decreased due to the enrichment of alloying elements in the intercritical annealing.[25] Therefore, as indicated in Figure 1, the second reverted transformation occurred at a lower temperature ($A_{c1}'$). When the intercritical tempering was conducted at a temperature between $A_{c1}'$ and $A_{c1}$, the second reverted austenite was formed at element-enriched region and dislocations, accompanying further enrichment of austenite stabilizers. As a result, more austenite is observed in Figure 3(d). This demonstrated that the intercritical annealing process was beneficial to
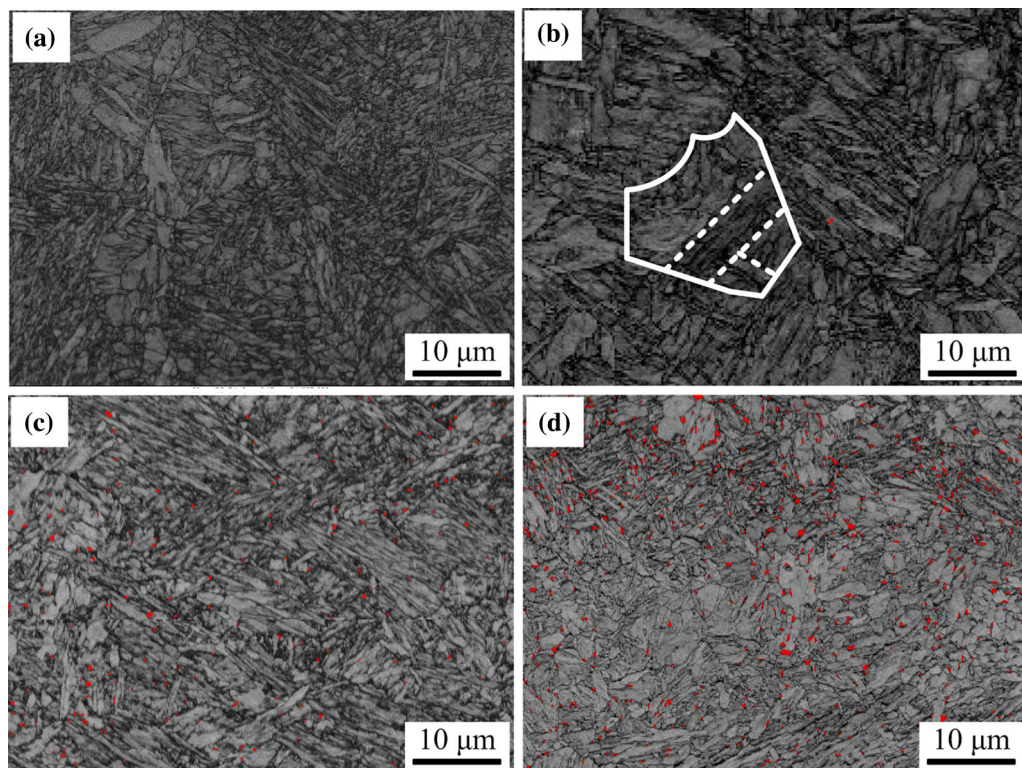


Fig. 3—EBSD images of steels subjected to various heat treatments: (a) as quenched; (b) T620; (c) IA700; (d) IA700-IT620. The red part corresponds to FCC retained austenite (Color figure online).

forming a higher volume fraction of the retained austenite. Alloying element-enriched retained austenite and martensite formed in the intercritical annealing process acted as preferential nucleation sites for the second reversed austenite during the tempering process. In addition, when we compared the BC maps of the T620 and IA700-IT620 steels as indicated in Figures 3(b) and (d), the characteristic packet and block substructures of lath martensite are visible within a prior austenite grain in Figure 3(b). However, substantial refinement occurred in the IA700-IT620 in which it was difficult to distinguish blocks and packets in the BC map (Figure 3(d)). Considering that the samples subjected to two heat treatment conditions were taken from the same as-quenched sample, the average prior austenite gain size was the same ~ 21 $\mu$m. Therefore, it can be reasonably considered that the microstructure was further refined by the intercritical annealing, which was consistent with the result in a previous study.[26]

Volume fractions of the retained austenite were quantitatively studied by using XRD analysis. Figure 4 shows the XRD spectra for the steels subjected to various heat treatments. For the as-quenched steel, no retained austenite was detected by XRD. When the as-quenched steel was directly tempered at 620 °C, the volume fraction of retained austenite was ~ 0 pct. This indicated that the retained austenite cannot be introduced to this steel merely by tempering. For IA700 steel, however, the volume fraction of retained austenite was ~ 8 pct. By using the second step of tempering at 620 °C, the volume fraction of retained austenite was further increased to ~ 15 pct, which was consistent with the EBSD results.

## B. Mechanical Properties

### 1. Tensile behavior

The mechanical behaviors in terms of strength, $Y/T$ ratio, and total elongation are listed in Table I for this Cu-containing steel after different heat treatments, and the corresponding engineering stress–strain curves and work hardening curves are presented in Figure 5. The quenched steel exhibited higher yield strength (980 MPa), ultrahigh tensile strength (1287 MPa), and lower $Y/T$ ratio (0.76), but a lower ductility (total elongation: 13.2 pct). When the quenched steel was subjected to direct tempering at 893 K (620 °C), there was negligible change in yield strength, while the tensile strength dropped dramatically, as depicted in Figure 5(a). This was attributed to microstructure recovery during tempering. The tensile strength was determined by the strength of soft phase and martensite according to the rule of mixture, while the yield strength was a result of precipitation strengthening and tempering softening.[27] During tempering, the supersaturated carbon in martensite precipitated and the dislocations reduced, leading to a dramatic drop in tensile strength. With regard to yield strength, the precipitation strengthening including Cu-rich particles and carbonitride compensated for the loss in yield strength caused by tempering softening, resulting in a negligible change. As a consequence, the $Y/T$ ratio increased up to 0.98. Furthermore, there existed yielding and slight work hardening due to the pile-up of the dislocations. In contrast, when an intercritically annealing at 973 K (700 °C) was exerted on the quenched steel, a much lower yield strength of 680 MPa and an ultrahigh tensile strength of 1012 MPa were achieved. This was attributed to the presence of dual-phase structure of ferrite and martensite. From Figure 5(b), one could not notice the work hardening resulted from TRIP effect, which indicated that 8.0 vol. pct of retained austenite obtained by intercritical annealing could not produce obvious TRIP effect. When the intercritically annealed steel was tempered at 893 K (620 °C), a better combination of strength and ductility was obtained. Compared to the steel subjected to conventional quenching and tempering, the additionally intercritical annealing led to a slight decrease in tensile strength (961 MPa), a dramatic decrease in yield strength (830 MPa) and a sharp increase in total elongation (22.2 pct). What is more, a considerably lower $Y/T$ ratio of 0.86 was obtained. The engineering stress–strain curve during tensile deformation is presented in Figure 5(a), which exhibited continuous yielding with observable yield point, indicative of a lower density of mobile dislocations. This would account for the decrease of yield strength in the IA700-IT620 steel. In addition, as indicated in Figure 5(a), an apparent work hardening was observed in the IA700-IT620 steel. The observations were further verified by the work hardening curves in Figure 5(b). A higher work hardening rate was obtained in the steel after intercritical annealing and tempering. This implied that the transformation of retained austenite contributed to the different work hardening rates in
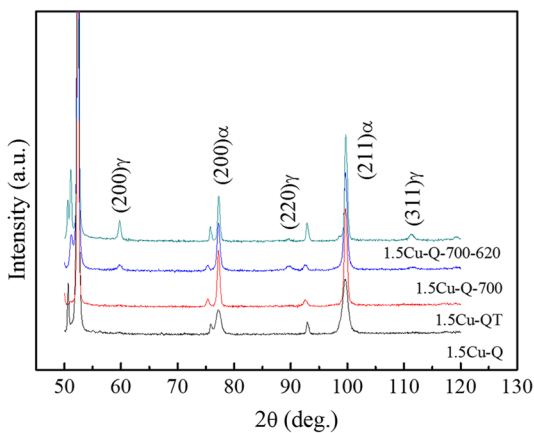


Fig. 4—XRD spectra of the steels subjected to various heat treatments.

**Table I. Tensile Properties of the Steels Subjected to Various Heat Treatments**

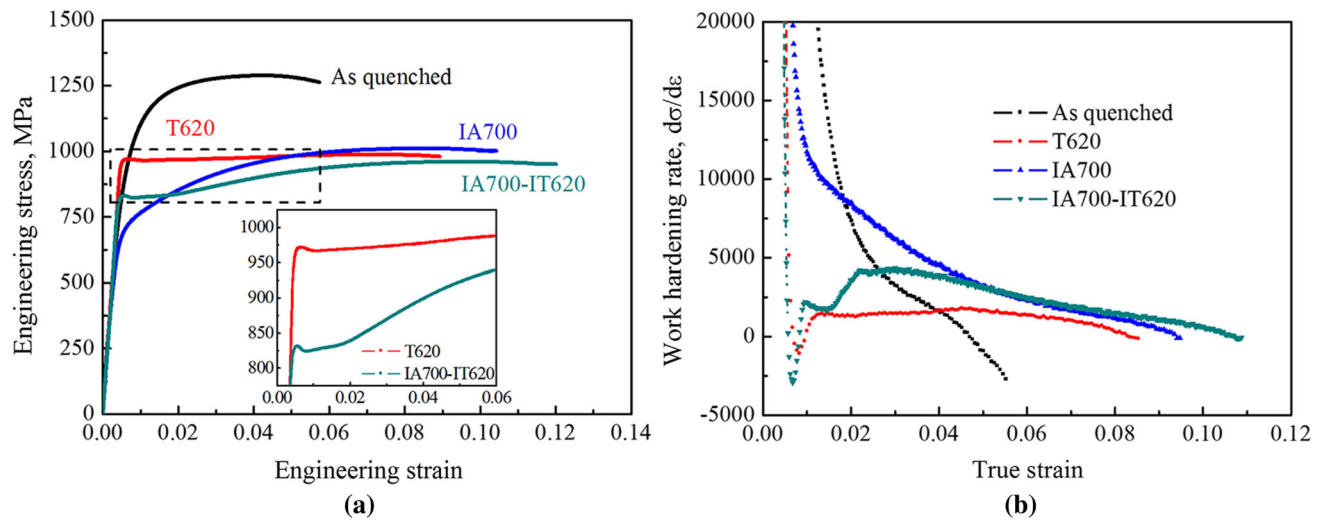| Steel | YS (MPa) | TS (MPa) | $Y/T$ ratio | TEL (Pct) |
|---|---|---|---|---|
| As-quenched | 980 | 1287 | 0.76 | 13.2 |
| T620 | 970 | 988 | 0.98 | 19.2 |
| IA700 | 680 | 1012 | 0.67 | 18.1 |
| IA700-IT620 | 830 | 961 | 0.86 | 22.2 |

Fig. 5—Engineering stress–strain curves (*a*) and work hardening curves (*b*) for the steels subjected to various heat treatments.

Table II.  Variation of the Charpy Impact Energy with Temperature for the IA700-IT620 and T620 Steels

| Steel | 288 K (15 °C) | 233 K (− 40 °C) | 193 K (− 80 °C) | 153 K (− 120 °C) | 77 K (− 196 °C) |
|---|---|---|---|---|---|
| T620 | 200 | 197 | 186 | 89 | 12 |
| IA700-IT620 | 220 | 219 | 209 | 183 | 50 |

addition to the dislocations. Thus, the tensile strength of the IA700-IT620 steel showed no obvious decline in comparison with the T620 steel. The enhanced ductility of the IA700-IT620 steel was resulted from the dynamic strain partitioning in austenite-martensite structure.[28]

### 2. Low-temperature toughness

The Charpy impact energy values for IA700-T620 and T620 steels tested at temperatures ranging from 77 K to 288 K (− 196 °C to 15 °C) are listed in Table II, and the corresponding variation curves of Charpy impact absorbed energy as a function of test temperature are plotted in Figure 6.

The IA700-IT620 steel showed higher impact energies regardless of test temperature, especially at temperature lower than 193 K (− 80 °C). Both of the steels exhibited a drop in the impact energy with decreasing temperature from 288 K to 77 K (15 °C to − 196 °C). It is worth noting that the T620 steel experienced a dramatic impact energy decrease to 89 J at 153 K (− 120 °C), while the IA700-T620 still remained a high level of 183 J. To obtain ductile-brittle transition temperature (DBTT), here the DBTT is defined as the temperature at which half of the upper shelf energy is reached in the impact test,[29] as demonstrated in Figure 6. Compared to the DBTT of 157 K (− 116 °C) for T620 steel, a lower DBTT of 109 K (− 164 °C) was achieved for the IA700-IT620 steel.

In order to further analyze the fracture features, SEM was used to observe the morphologies of the fractured surfaces as shown in Figure 7. Figures 7(a), (b), and (c) show the surface morphologies of the IA700-IT620 steel fractured at 233 K, 153 K, and 77 K (− 40 °C, − 120 °C and − 196 °C), respectively. From Figures 7(a)

and (b), we can see that the surface morphology of the IA700-IT620 steel impact fractured at 233 K and 153 K (− 40 °C and − 120 °C) is of ductile characteristic with larger dimples. When the temperature was decreased to 77 K (− 196 °C), quasi-cleavage fracture with some small dimples can be observed as indicated in Figure 7(c). Figures 7(d), (e), and (f) show the surface morphology of the T620 steel fractured at 233 K, 153 K, and 77 K (− 40 °C, − 120 °C and − 196 °C), respectively. When the T620 steel was impacted fractured at 233 K (−40 °C), the surface morphology with smaller dimples was observed as seen from Figure 7(d). Figure 7(e) is the SEM surface morphology of the T620 steel fractured at 153 K (− 120 °C), which behaves complete cleavage fracture with relatively smaller cleavage facets and the cracks transgranularly propagated into matrix. At 77 K (− 196 °C), the size of cleavage facets for the T620 steel appeared to be much larger, indicative of long straight crack propagation paths.

Therefore, excellent low-temperature toughness was obtained in the IA700-IT620 steel. Through the intercritical annealing process, retained austenite was introduced to the IA700-IT620 steel, while the effective grain size was refined. They were considered to be the two reasons to significantly influence the low-temperature toughness.

### C. Toughening Mechanism

It has been found that a reduced average grain size generally leads to a lower DBTT and resultant higher low-temperature toughness.[30,31] The DBTT is believed to be the point at which yield stress is equal to the

fracture stress. Yield stress increases with the decrease of temperatures, but the fracture stress is independent of the temperature. Thus, a decrease in yield stress or an increase in fracture stress will make the DBTT shift to a lower temperature. However, the grain refinement contributes more significant increase to the fracture stress than the yield stress, and thus the DBTT goes

toward the lower temperature.[32,33] In the present study, the microstructure of IA700-IT620 steel was much finer than that of T620 steel, which led to a lower DBTT and increased low-temperature toughness.

From the point of crack initiation and propagation, Stoloff gave an equation describing the condition for plastically induced crack nucleation at a given temperature, which implied that any factors increasing $\sigma_i$, $k_y$, or $d$ would increase the tendency for brittle fracture.[32] In addition, by linear intercept method on SEM images in Figure 7, the arithmetic mean of the observed facet size was determined to be 8.8 and 12.2 $\mu m$ for the IA700-IT620 steel and T620 steel, respectively. This confirms that the facet size is reduced with the decrease of the effective grain size, which can lead to deflection of the crack propagation paths, and thus the low-temperature toughness was enhanced.

In addition to grain refinement produced by the intercritical annealing, the relationship between austenite and low-temperature toughness has been a controversial topic for a long time. It has been suggested that the austenite with high stability can maintain the TRIP effect at high strains, thereby reducing the average length of unit crack paths.[34] Thomas[35] suggested that stable retained austenite seemed to be beneficial to fracture toughness, because unstable austenite decomposed to form carbide during tempering, destroying the toughness. Therefore, it is essential to understand the stability of retained austenite.
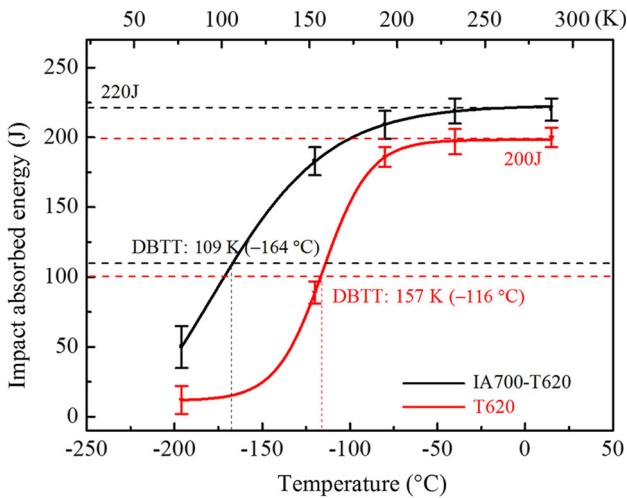


Fig. 6—Variation of Charpy impact absorbed energy as a function of temperature for the IA700-IT620 and T620 steels.
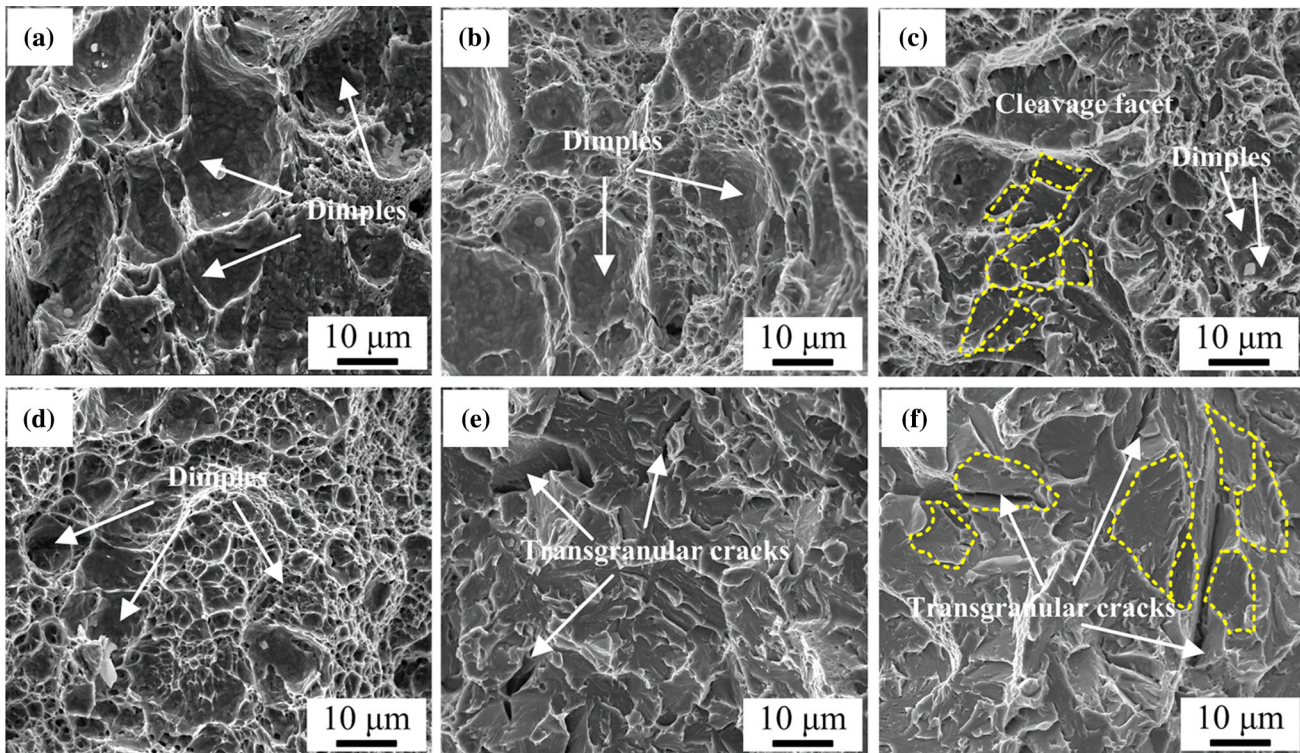


Fig. 7—SEM fractographs of the IA700-IT620 and T620 steels impact fractured at 233 K, 153 K, and 77 K (− 40 °C, − 120 °C, and − 196 °C): (a) IA700-IT620, 233 K (− 40 °C); (b) IA700-IT620, 153 K (− 120 °C); (c) IA700-IT620, 77 K (− 196 °C); (d) T620, 233 K (− 40 °C); (e) T620, 153 K (− 120 °C); (f) T620, 77 K (− 196 °C).

**Table III. Measured Chemical Compositions, Calculated SFE at Ambient Temperature, and Ms for IA700 and IA700-IT620 Steel**

|  | C (Mass Pct) | Mn (Mass Pct) | Ni (Mass Pct) | Cr (Mass Pct) | Cu (Mass Pct) | SFE (mJ/m$^2$) | Ms [K (°C)] |
|---|---|---|---|---|---|---|---|
| IA700 | 0.721 | 1.01 | 2.88 | 1.28 | 1.25 | 40.3 | 395 (122) |
| IA700-IT620 | 0.778 | 1.74 | 3.64 | 1.30 | 0.96 | 43.4 | 324 (51) |

The thermal stability of austenite is affected not only by the driving force for the athermal $\alpha'$-martensitic transformation but also by the stacking fault energy (SFE).[36] Table III lists the chemical compositions of the austenite phase obtained by energy dispersive X-ray spectroscopy (EDXS) analysis, the corresponding room-temperature SFE calculated using the classic formula proposed by Brofman et al.,[37] and the martensite start transformation temperature (Ms) calculated by Eldis's Ms equation proposed in Gorni's handbook.[38] The carbon concentration $x_C$ of the retained austenite can be estimated using Eq. [2].[34] By comparison, the concentration of austenite stabilizers (C, Mn, Ni) for IA700-IT620 was higher than that of IA700, indicative of further enrichment of C, Mn, Ni during tempering, which was beneficial for austenite stabilization. Note that the SFE value was higher in IA700-IT620, which implied that the retained austenite possessed considerably high stability. Moreover, the Ms of IA700-IT620 was lower than that of IA700, further indicating the high stability of the retained austenite. Higher SFE and lower Ms would inhibit martensitic transformation by influencing the driving force for the athermal $\alpha'$-martensite transformation. Figure 8 shows the XRD spectra of the retained austenite for the steels subjected to subzero treatment. The volume fractions of the retained austenite were estimated to be 15, 13, and 8.9 pct at temperatures of 288 K, 153 K, and 77 K (15 °C, − 120 °C and − 196 °C), respectively. It can be inferred that the amount of retained austenite in the steels immersed in liquid nitrogen was slightly less than that in steels at 288 K (15 °C), indicating that the retained austenite was quite thermally stable. This experimental result is consistent with the theoretical analysis.

$$\partial_\gamma = 3.556 + 0.0453x_C + 0.00095x_{Mn} + 0.0056x_{Al}, \quad [2]$$

where the austenite lattice $\partial_\gamma$ is in Å, and $x_C$, $x_{Mn}$, and $x_{Al}$ are the concentrations of carbon, manganese, and aluminum, respectively, in wt pct.

As shown in Figure 9(a), in order to reveal the mechanical stability of the retained austenite in the IA700-IT620 steel, the amount of retained austenite after the impact test at 153 K (− 120 °C) was measured and analyzed by XRD. The volume fraction of retained austenite as a function of the distance away from the fractured surface is plotted in Figure 9(b). It can be seen from Figure 9(a) that there were obvious austenite diffraction peaks at the distance of 9, 7, 5, 3 mm away from the fractured surface. The volume fractions of retained austenite were estimated to be 13, 12.8, 10.7, and 10 pct, respectively, remaining almost the same level. Nevertheless, the austenite diffraction peaks at the distance of 1 mm were extremely weak. The volume
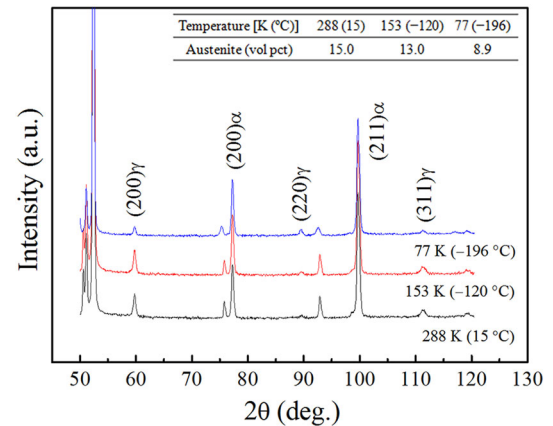


Fig. 8—XRD spectra for the IA700-IT620 steel treated at different temperatures.

fraction of the retained austenite sharply decreased to nearly 0 pct. This suggested the occurrence of the deformation-induced transformation near the fracture surface. Therefore, it is reasonable to deduce that the enhanced low-temperature toughness is related to TRIP effect of the retained austenite. As indicated in Figure 10, the EBSD images of the retained austenite at different locations away from the fracture surface of the IA700-IT620 steel further confirmed the result. Figure 10(a) displays the distribution of the retained austenite at the distance of 7 mm away from the fracture surface. One may observe that the retained austenite was dispersedly distributed in the matrix and between boundaries. At the distance of 3 mm away from the fracture surface (Figure 10(b)), the amount of retained austenite exhibited a decrease, indicating that a part of retained austenite transformed to martensite. A low band contrast (BC) between boundaries also confirmed the occurrence of martensite transformation. At the distance of 1 mm away from the fracture surface (Figure 10(c)), however, only a trace amount of retained austenite is present. Also, more regions with low BC were obtained, which was believed to correspond to martensite transformed from retained austenite during impact test. This is consistent with the XRD results. It has been reported that the stability of retained austenite is proportional to the absorbed energy for the crack propagation.[39] Therefore, it is evident that the phase stability of retained austenite affects the impact.

In this study, the mechanism of crack initiation and propagation can be employed to elucidate the improved low-temperature toughness caused by grain refinement and stable retained austenite. Firstly, grain refinement caused by intercritical annealing increased the amount
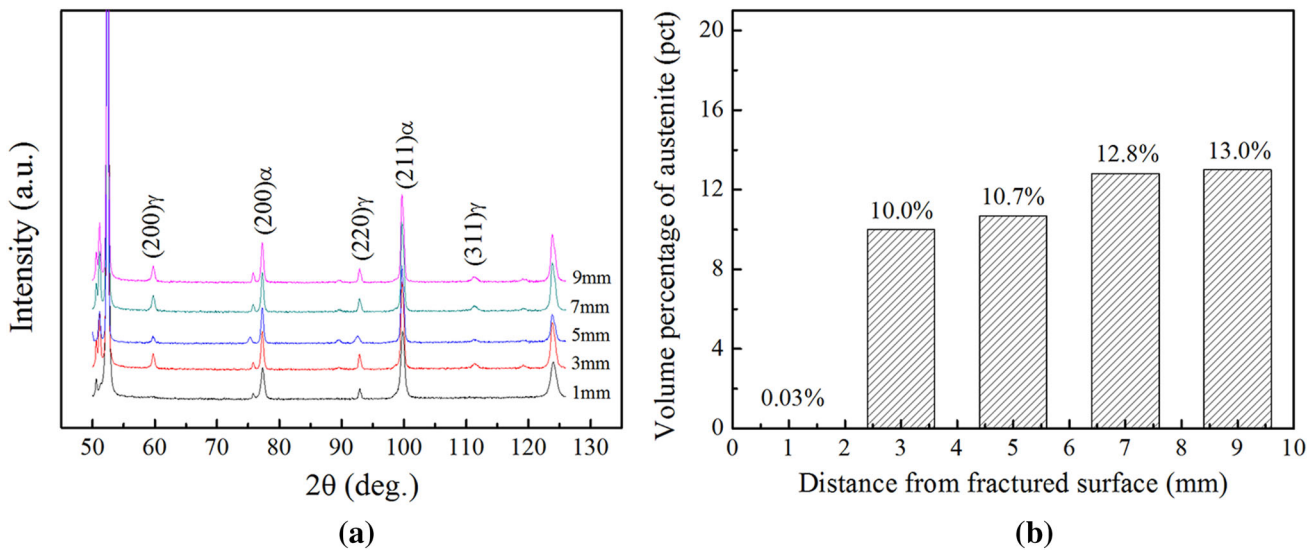
Fig. 9—XRD spectra (*a*) and measured austenite volume fractions (*b*) of different locations away from the fractured surface of the IA700-IT620 steel tested at 153 K (− 120 °C).
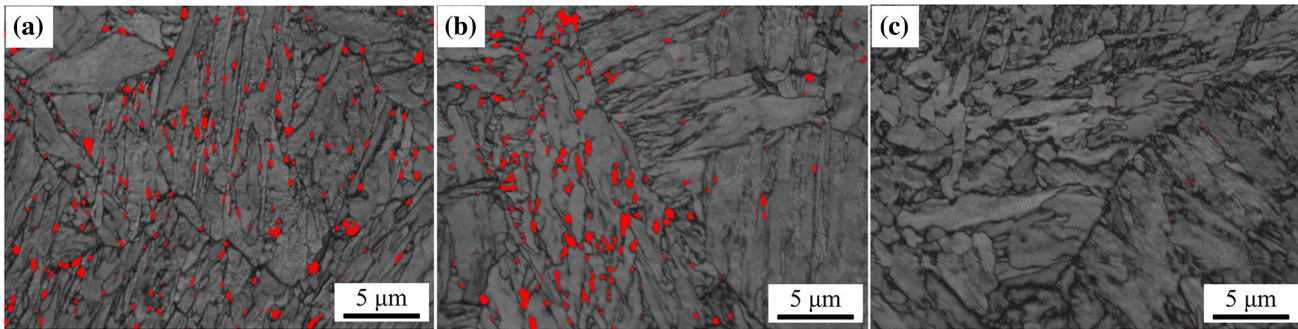


Fig. 10—EBSD analysis of the retained austenite at different locations away from the fracture surface of the IA700-IT620 steel tested at 153 K (− 120 °C) (*a*) 7 mm, (*b*) 3 mm, (*c*) 1 mm.

of high-angle grain boundaries and thus deflected the crack propagation paths. Secondly, the retained austenite existed at low temperature due to its highly thermal stability. During the impact test, the retained austenite transformed to the martensite, which relieved the local stress concentration and delayed the initiation of the crack.[40] Moreover, during the crack propagation, the martensite formed at the tip of the crack propagation suppressed the crack propagation. Thus, enhanced low-temperature toughness was obtained.

## IV. CONCLUSIONS

A novel intercritical annealing heat treatment has been introduced to a Fe-C-Mn-Ni-Cu structural steel. Microstructure and mechanical properties of this steel with intercritical annealing have been characterized and compared with those of steels with conventional quenching and tempering heat treatment. The following conclusions can be drawn.

1. A mixed microstructure consisting of intercritical ferrite, tempered martensite, and some amount of retained austenite was obtained in a low-carbon lean-alloyed steel by applying intercritical annealing in the conventional quenching and tempering treatment. Also, the microstructure can be further refined by the reversed transformation during intercritical annealing process. Both of them are beneficial to the good combination of strength, ductility, and toughness.

2. After intercritical annealing heat treatment, the yield strength and ultimate tensile strength were above 800 MPa and 900 MPa for the Fe-C-Mn-Ni-Cu structural steel, respectively. The total elongation and *Y*/*T* ratio were measured to be 22.2 pct and 0.86, respectively. This could be related with multi-phase microstructure and deformation-induced transformation of the retained austenite during tensile deformation.

3. The steel with intercritical annealing showed excellent low-temperature toughness, with average

Charpy impact energy of 183 J at 153 K (− 120 °C). This can be attributed to grain refinement and TRIP effect of the retained austenite *via* intercritical annealing heat treatment. Grain refinement led to a lower DBTT and increased low-temperature toughness. Also, a smaller cleavage facet size was obtained along with grain refinement, which can improve low-temperature toughness *via* deflection of crack propagation paths. On the other hand, thermal stable austenite transformed to martensite during low-temperature impact, which improved low-temperature toughness by changing absorbed energy of crack initiation and propagation.

## REFERENCES

1. K. Otani, H. Muraoka, S. Tsuruta, K. Hattori, and H. Kawazoe: *Nippon Steel Tech. Rep.*, 1993, vol. 58, pp. 1–8.
2. D. Liu, Q. Li, and T. Emi: *Metall. Mater. Trans. A*, 2010, vol. 42A, pp. 1349–61.
3. H.B. Liu, H.Q. Zhang, and J.F. Li: *Int. J. Press. Vessel. Pip.*, 2018, vol. 168, pp. 200–09.
4. G.K. Tirumalasetty, M.A. van Huis, C.M. Fang, Q. Xu, F.D. Tichelaar, D.N. Hanlon, J. Sietsma, and H.W. Zandbergen: *Acta Mater.*, 2011, vol. 59, pp. 7406–15.
5. Y. Funakawa, T. Shiozaki, K. Tomita, T. Yamamoto, and E. Maeda: *ISIJ Int.*, 2004, vol. 44, pp. 1945–51.
6. M.Y. Chen, M. Gouné, M. Verdier, Y. Bréchet, and J.R. Yang: *Acta Mater.*, 2014, vol. 64, pp. 78–92.
7. S. Vaynman, D. Isheim, R. PrakashKolli, S.P. Bhat, D.N. Seidman, and M.E. Fine: *Metall. Mater. Trans. A*, 2008, vol. 39A, pp. 363–73.
8. Y. Zhou, J. Chen, Y. Xu, and Z. Liu: *J. Mater. Sci. Technol.*, 2013, vol. 29, pp. 168–74.
9. Y. Zhou, T. Jia, X. Zhang, Z. Liu, and R.D.K. Misra: *Mater. Sci. Eng. A*, 2015, vol. 626, pp. 352–61.
10. H. Tagawa, T. Taira, K. Ume, and T. Ishihara: *Offshore Technology Conference*, Texas, Houston, 1981, pp. 235–43.
11. Z.J. Xie, Y.P. Fang, Y. Cui, X.M. Wang, C.J. Shang, and R.D.K. Misra: *Mater. Sci. Technol.*, 2016, vol. 32, pp. 691–96.
12. A. Nagao, T. Ito, and T. Obinata: *JFE Tech. Rep.*, 2008, vol. 11, pp. 13–18.
13. C. Sun, S.L. Liu, R.D.K. Misra, Q. Li, and D.H. Li: *Mater. Sci. Eng. A*, 2018, vol. 711, pp. 484–91.
14. S.P. Rawal and J. Gurland: *Metall. Trans. A*, 1977, vol. 8A, pp. 691–98.
15. Y. Nagai, H. Fukami, H. Inoue, A. Date, T. Nakashima, A. Kojima, and A. Toshihiko: *Nippon Steel Tech. Rep.*, 2004, vol. 90, pp. 14–19.
16. D. Liu, B. Cheng, and M. Luo: *ISIJ Int.*, 2011, vol. 51, pp. 603–11.
17. P. Movahed, S. Kolahgar, S.P.H. Marashi, M. Pouranvari, and N. Parvin: *Mater. Sci. Eng. A*, 2009, vol. 518, pp. 1–6.
18. J. Shi, X. Sun, M. Wang, W. Hui, H. Dong, and W. Cao: *Scripta Mater.*, 2010, vol. 63, pp. 815–18.
19. J.I. Kim, C.K. Syn, and J.W. Morris: *Metall. Trans. A*, 1983, vol. 14A, pp. 93–103.
20. R.L. Miller: *Metall. Mater. Trans. B*, 1972, vol. 3B, pp. 905–12.
21. J. Hu, L. Du, W. Xu, J. Zhai, Y. Dong, Y. Liu, and R.D.K. Misra: *Mater. Charact.*, 2018, vol. 136, pp. 20–28.
22. J. Chiang, B. Lawrence, J.D. Boyd, and A.K. Pilkey: *Mater. Sci. Eng. A*, 2011, vol. 528, pp. 4516–21.
23. W.H. Zhou, V.S.A. Challa, H. Guo, C.J. Shang, and R.D.K. Misra: *Mater. Sci. Eng. A*, 2015, vol. 620, pp. 454–62.
24. Z.J. Xie, G. Han, W.H. Zhou, C.Y. Zeng, and C.J. Shang: *Mater. Charact.*, 2016, vol. 113, pp. 60–66.
25. Z.J. Xie, S.F. Yuan, W.H. Zhou, J.R. Yang, H. Guo, and C.J. Shang: *Mater. Des.*, 2014, vol. 59, pp. 193–98.
26. H. Shirazi, G. Miyamoto, S. Hossein Nedjad, H. Ghasemi Nanesa, M. Nili Ahmadabadi, and T. Furuhara: *J. Alloys Compd.*, 2013, vol. 577, pp. S572–S77.
27. S. Wang, H. Yu, H. Gu, T. Zhou, and L. Wang: *Mater. Sci. Eng. A*, 2019, vol. 744, pp. 299–304.
28. D. Liu, L.X. Du, J. Hu, H.Y. Wu, X.H. Gao, and R.D.K. Misra: *J. Alloys Compd.*, 2017, vol. 695, pp. 2072–82.
29. R. Song, D. Ponge, and D. Raabe: *Acta Mater.*, 2005, vol. 53, pp. 4881–92.
30. T. Hanamura, F. Yin, and K. Nagai: *ISIJ Int.*, 2004, vol. 44, pp. 610–17.
31. R. Song, D. Ponge, D. Raabe, J.G. Speer, and D.K. Matlock: *Mater. Sci. Eng. A*, 2006, vol. 441, pp. 1–17.
32. N.S. Stoloff: *Chapter 1-Effects of alloying on fracture characteristics*, Elsevier Inc., Amsterdam, 1969, pp. 1–81.
33. N.J. Petch: Proceedings of an International Conference on the Atomic Mechanisms of Fracture, Swampscott, Mass, 1959, pp. 54–64.
34. G. Gao, H. Zhang, X. Gui, P. Luo, Z. Tan, and B. Bai: *Acta Mater.*, 2014, vol. 76, pp. 425–33.
35. G. Thomas: *Metall. Trans. A*, 1978, vol. 9A, pp. 439–50.
36. T. Masumura, N. Nakada, T. Tsuchiyama, S. Takaki, T. Koyano, and K. Adachi: *Acta Mater.*, 2015, vol. 84, pp. 330–38.
37. P.J. Brofman and G.S. Ansell: *Metall. Mater. Trans. A*, 1978, vol. 9A, pp. 879–80.
38. A.A. Gorni: *Steel Forming and heat treating handbook*, São Vicente SP, Brazil, 2015.
39. M.T. Kim, T.M. Park, K.H. Baik, W.S. Choi, P.P. Choi, and J. Han: *Acta Mater.*, 2019, vol. 164, pp. 122–34.
40. B. Fultz, J.I. Kim, Y.H. Kim, H.J. Kim, G.O. Fior, and J.W. Morris: *Metall. Trans. A*, 1985, vol. 16A, pp. 2237–49.